Classifying Topology in Photonic Heterostructures with Gapless Environments

Kahlil Y. Dixon,[1,*] Terry A. Loring,[2] and Alexander Cerjan[1,†]
[1]Center for Integrated Nanotechnologies, Sandia National Laboratories, Albuquerque, New Mexico 87185, USA
[2]Department of Mathematics and Statistics, University of New Mexico, Albuquerque, New Mexico 87131, USA

(Received 31 March 2023; accepted 18 October 2023; published 22 November 2023)

Photonic topological insulators exhibit bulk-boundary correspondence, which requires that boundary-localized states appear at the interface formed between topologically distinct insulating materials. However, many topological photonic devices share a boundary with free space, which raises a subtle but critical problem as free space is gapless for photons above the light line. Here, we use a local theory of topological materials to resolve bulk-boundary correspondence in heterostructures containing gapless materials and in radiative environments. In particular, we construct the heterostructure's spectral localizer, a composite operator based on the system's real-space description that provides a local marker for the system's topology and a corresponding local measure of its topological protection; both quantities are independent of the material's bulk band gap (or lack thereof). Moreover, we show that approximating radiative outcoupling as material absorption overestimates a heterostructure's topological protection. As the spectral localizer is applicable to systems in any physical dimension and in any discrete symmetry class (i.e., any Altland-Zirnbauer class), our results show how to calculate topological invariants, quantify topological protection, and locate topological boundary-localized resonances in topological materials that interface with gapless media in general.

DOI: 10.1103/PhysRevLett.131.213801

Recent advances in topological photonics [1–3] have led to the development of novel technologies including topological lasers [4–12] and devices that create and route quantum light [13–20]. However, the utility of many of these devices is predicated on the presence of, and potential coupling to, scattering channels in the surrounding environment that are degenerate with the boundary-localized topological states that underpin these devices' functionality. Thus, even though these devices can feature photonic crystals or other lattices with complete topological band gaps in their interior, their boundary-localized states are generally resonances, not bound modes, that radiate into the surrounding environment as free space is gapless above the light line.

Unfortunately, the fact that the typical environment for topological photonic structures is gapless, rather than gapped (i.e., insulating), presents a fundamental challenge to our understanding of these devices. Heuristically, topological boundary-localized modes form at the interface between two gapped materials with different bulk invariants as a resolution to the need for band continuity across the heterostructure's interface; the band gap must close in the vicinity of the interface so that the different bulk invariants can be reconciled, yielding interface-localized states [1] [Fig. 1(a)]. Indeed, traditional approaches to material topology have been highly successful at predicting the interface phenomena in heterostructures featuring topologically nontrivial insulators [3,21–24] and semimetals [25–37]. But, if at least one of the materials in a heterostructure is gapless, this explanation fails, as the band gap must close in the vicinity of the interface regardless (so as to satisfy bulk band continuity between the two materials); any need to reconcile different bulk material topologies could occur as part of this standard band closing process without resulting in topological interface-localized states or resonances [Fig. 1(b)]. Note, in this context "gapless" specifically refers to a d-dimensional material with $(d-1)$-dimensional isofrequency contours over a given range of wavelengths (i.e., those wavelengths in the other material's bulk band gap). Thus, the plethora of photonic experiments that have observed topological boundary-localized resonances in devices that abut and radiate to free space suggests that material topology must be definable in heterostructures

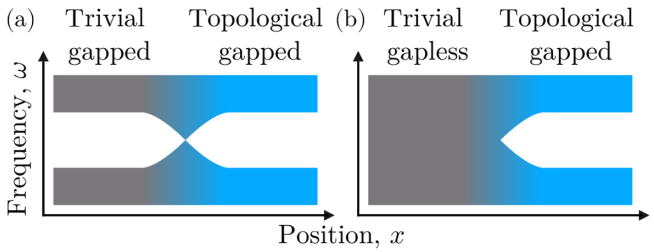

FIG. 1. (a) Schematic of the local density of states as the probed position is varied across the interface of a heterostructure formed by a trivial insulator and topological insulator with a common bulk band gap. (b) A similar schematic, except in which the trivial material is gapless.

containing a gapless material, even if the lack of a global bulk band gap prohibits the use of traditional theories of physical topology.

Here, we identify topological boundary-localized resonances and quantify their protection in gapless heterostructures with radiative environments using a theory of topological materials based on their real-space description. To do so, we construct the heterostructure's spectral localizer, a composite operator that combines a system's Hamiltonian and position operators with a Clifford representation, and which provides local topological markers and a spatially resolved measure of protection even for non-Hermitian systems. We demonstrate this topological classification approach on a 2D photonic Chern crystal embedded in free space with radiative boundary conditions. Using this model, we also show that radiative losses and material absorption have qualitatively different consequences for a system's topological protection, and approximating radiative outcoupling as absorption will substantially overestimate the protection of the boundary-localized resonances. Finally, we provide an example of how topological robustness against system disorder manifests in this real-space classification approach. Our results reveal that bulk-boundary correspondence persists in gapless heterostructures, providing a rigorous framework for understanding many types of topological photonic devices.

We begin by considering a prototypical topological photonic system consisting of a photonic Chern insulator embedded in free space. In particular, we use a finite portion of the 2D magneto-optic photonic crystal proposed by Haldane and Raghu [38,39] surrounded on all sides by vacuum, with the radiative boundary condition implemented using stretched-coordinate perfectly matched layers (PML) [40] [Fig. 2(a)]. When an external magnetic field is applied, a topologically nontrivial band gap opens in the photonic crystal's transverse electric (TE) sector that supports chiral edge modes within this gap [Fig. 2(b)]. As the photonic crystal in our model system is finite, all of its states, including its chiral edge modes, are resonances as they decay due to radiative outcoupling. These chiral edge resonances can be seen in the system's local density of states within the bulk band gap of the photonic Chern insulator [Fig. 2(c)]. Altogether, this model system preserves all of the salient features of many topological photonic systems that have been previously experimentally observed [41,42], but whose topological protection cannot be quantified using topological band theory because the materials that form the heterostructure lack a common bulk band gap.

Instead, to show that the gapless heterostructure in Fig. 2(a) must possess protected boundary-localized resonances due to the nontrivial topology of the central lattice, we employ the spectral localizer [43–45]. For a d-dimensional system, the spectral localizer is a composite operator that combines the system's Hamiltonian H and position operators $X_1, X_2, \ldots, X_d$ using a nontrivial Clifford representation, and yields both a local topological marker and local measure of protection. For the non-Hermitian 2D

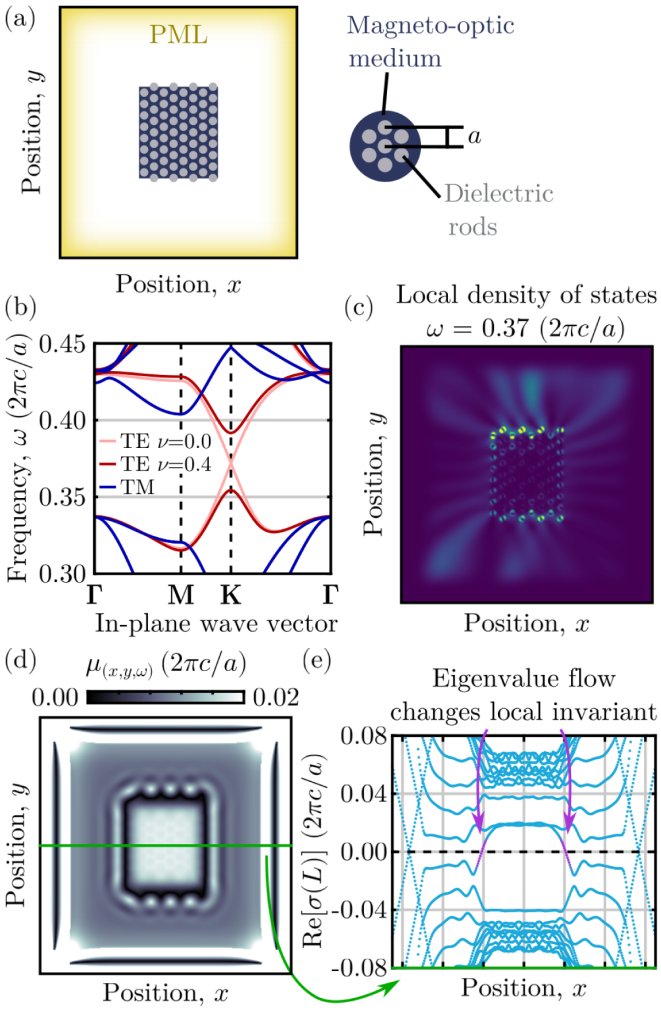

FIG. 2. (a) Schematic of a 2D photonic Chern insulator embedded in free space $\varepsilon_{\text{fs}} = 1$ with radiative boundary conditions. The topological photonic insulator is composed of dielectric rods $\varepsilon_{\text{rod}} = 14$ with spacing a in a magneto-optic background $\varepsilon_{\text{mo}} = \left(\begin{smallmatrix} 1 & -i\nu \\ i\nu & 1 \end{smallmatrix}\right)$. (b) Bulk band structure for the photonic Chern insulator for the TE modes with $\nu = 0$ (light red) and $\nu = 0.4$ (dark red), and the transverse magnetic (TM) modes that are independent of ν. (c),(d) Local density of states (c) and local gap $\mu_{(x,y,\omega)}$ (d) for the finite system at $\omega = 0.37(2\pi c/a)$, shown on the same spatial scale as (a). (e) Spectral flow of the real parts of the 20 eigenvalues of $L_{(x,y,\omega)}$ closest to 0 for y fixed to the center of the finite system [green line in (d)], and at $\omega = 0.37(2\pi c/a)$. (d) and (e) are calculated using $\kappa = 0.04(2\pi c/a^2)$.

system that we consider here, we can use the Pauli matrices as the Clifford representation [as they generate a representation of $\mathcal{C}\ell_3(\mathbb{C})$] to write the spectral localizer as [46]

$$L_{(x,y,\omega)}(X, Y, H) = \begin{pmatrix} H - \omega I & \kappa(X - xI) - i\kappa(Y - yI) \\ \kappa(X - xI) + i\kappa(Y - yI) & -(H - \omega I)^{\dagger} \end{pmatrix}. \tag{1}$$

Here, x, y, ω are the choices of position and frequency where the spectral localizer is evaluated, X and Y are the 2D position operators, I is the identity matrix, and κ is a positive scaling coefficient with units of frequency times inverse distance.

Intuitively, the spectral localizer can be viewed as a composition of the eigenvalue equations [such as $(H-\omega I)|\psi\rangle = 0$] of the (generally) noncommuting operators X, Y, H using the Pauli matrices. Despite the lack of a joint spectrum for X, Y, H, the spectral localizer can be used to determine whether a given choice of x, y, ω yields an approximate joint eigenvector of X, Y, H, i.e., is there some vector $|\phi\rangle$ for which $H|\phi\rangle \approx \omega|\phi\rangle$, $X|\phi\rangle \approx x|\phi\rangle$, and $Y|\phi\rangle \approx y|\phi\rangle$ [47]. A measure of how good these approximations are is given by

$$\mu_{(x,y,\omega)}(X,Y,H) = \min\left(|\mathrm{Re}\{\sigma[L_{(x,y,\omega)}(X,Y,H)]\}|\right), \quad (2)$$

i.e., the minimum distance over all of the eigenvalues of $L_{(x,y,\omega)}$ from the imaginary axis, where $\sigma(L)$ is the spectrum of L. Smaller values of $\mu_{(x,y,\omega)}$ indicate that x, y, ω are closer to yielding a joint eigenvector of X, Y, H. However, even if $\mu_{(x,y,\omega)}(X,Y,H) = 0$, these approximations do not become exact (noncommuting operators generally cannot be even partially simultaneously diagonalized) [43,47].

A physical picture of the spectral localizer's connection to material topology can be built from the behavior of atomic limits. In an atomic limit, $[H^{(\mathrm{AL})}, X_j^{(\mathrm{AL})}] = 0$, which stems from the system's Wannier functions being localized to a single lattice site [48]. This commutation relation, coupled with the fact that position operators commute $[X_j, X_l] = 0$, requires the eigenvalues of $L_{(x,y,\omega)}$ to be equally partitioned between having positive and negative real parts for any choice of x, y, ω. In other words, for atomic limits $\mathrm{sig}[L_{(x,y,\omega)}] = 0$, where sig denotes a matrix's signature, its number of eigenvalues with positive real parts minus its number with negative real parts [49]. However, just as 0D systems can be topologically classified based on the number of eigenvalues they possess above and below a specified band gap [50], 2D systems can be locally classified based on the partitioning of the spectrum of $L_{(x,y,\omega)}$, assuming that $\mu_{(x,y,\omega)} > 0$ [43].

Thus, if a generic system with $[H, X_j] \neq 0$ has $\mathrm{sig}[L_{(x,y,\omega)}] = 0$, then it is continuable to an atomic limit via a path of invertible matrices for that choice of x, y, ω, i.e., the system is locally topologically trivial. Conversely, if $\mathrm{sig}[L_{(x,y,\omega)}] \neq 0$, there is an obstruction to finding such a path, and the system is topologically nontrivial at that x, y, ω. As this classification approach is not restricting the matrix continuation path to preserve any system symmetries, the signature of $L_{(x,y,\omega)}$ defines a local Chern marker [43,46],

$$C^{\mathrm{L}}_{(x,y,\omega)}(X,Y,H) = \frac{1}{2}\mathrm{sig}[L_{(x,y,\omega)}(X,Y,H)] \in \mathbb{Z}. \quad (3)$$

For semi-infinite Hermitian systems, $C^{\mathrm{L}}_{(x,y,\omega)}$ is provably equal to the Chern number [45]. Moreover, as the partitioning of the spectrum of $L_{(x,y,\omega)}$ cannot change without $\mu_{(x,y,\omega)} = 0$, $\mu_{(x,y,\omega)}$ is a measure of the topological protection in a system and can be thought of as a "local band gap."

Altogether, the spectral localizer can be understood as a method for performing dimensional reduction consistent with Bott periodicity [43]. After dimensional reduction, the local invariants for all ten discrete symmetry classes (i.e., Altland-Zirnbauer classes [51–53]) become essentially one of the three invariants introduced by Kitaev [50]: matrix signatures for $\mathbb{Z}$ invariants, or signs of determinants or signs of Pfaffians for $\mathbb{Z}_2$ invariants. Additionally, one can consider $L_{(x,y,\omega)}$ to be the Hamiltonian of a modified system, enabling the local gap and local index to be experimentally observed [54].

To apply the spectral localizer to the photonic crystal heterostructure considered in Fig. 2(a), we first reformulate Maxwell's equations into a Hamiltonian, with

$$H(\mathbf{x}) = M^{-1/2}(\mathbf{x}) W M^{-1/2}(\mathbf{x}),$$
$$W = \begin{pmatrix} 0 & -i\nabla\times \\ i\nabla\times & 0 \end{pmatrix}, \text{ and } M(\mathbf{x}) = \begin{pmatrix} \bar{\bar{\mu}}(\mathbf{x}) & 0 \\ 0 & \bar{\bar{\varepsilon}}(\mathbf{x}) \end{pmatrix}. \quad (4)$$

In doing so, we are assuming that the frequency dependence of the permittivity $\bar{\bar{\varepsilon}}$ and permeability $\bar{\bar{\mu}}$ tensors can be neglected over the frequency range of interest, and that both are semipositive definite [55]. To use this Hamiltonian in Eq. (1), it must be discretized so that it becomes a bounded, finite matrix. Here, we use a 2D Yee grid [56]. The discretization scheme also defines the position operators X, Y, which in the basis of Eq. (4) are diagonal matrices whose elements $[X]_{jj}$ and $[Y]_{jj}$ correspond to the spatial coordinates of the jth vertex in the discretization. Note that the stretched-coordinate perfectly matched layers make W non-Hermitian.

Overall, the spectral localizer's numerical approach is similar to frequency-domain methods for solving Maxwell's equations because only a single frequency is considered within a given simulation. However, as Eq. (1) also requires specifying x, y for each simulation and $L_{(x,y,\omega)}$ is connected to the approximate joint eigenvectors of X, Y, H (i.e., their so-called multioperator pseudospectrum), the spectral localizer approach is better classified as a "pseudospectral-domain" method. Thus, our implementation of Eq. (1) is a finite-difference pseudospectral-domain method and is publicly available [57,58].

Applying the spectral localizer to the topological photonic system considered in Fig. 2(a) shows, that for frequencies within the topological band gap of the photonic

Chern crystal, the local gap $\mu_{(x,y,\omega)}$ closes around the boundary of the crystal, inside which the local Chern number becomes nontrivial $C^{\mathrm{L}}_{(x,y,\omega)} = 1$ [Fig. 2(d)]. Moreover, monitoring the spectrum of $L_{(x,y,\omega)}$ near zero as one of the coordinates is varied across the system (fixing the other coordinate and ω) reveals the lone eigenvalue of $L_{(x,y,\omega)}$ responsible for the change in the system's local Chern marker [Fig. 2(e)]. As locations where $\mu_{(x,y,\omega)} \approx 0$ indicate the presence of an approximate eigenstate of H (with eigenvalue near ω that is simultaneously approximately localized near x, y), the local gap closing around the topological photonic crystal is the manifestation of bulk-boundary correspondence in the spectral localizer framework. Thus, the spectral localizer demonstrates that the boundary-localized resonances observed in topological photonic systems embedded in free space stem from the topological material, and the nonzero localizer gap $[\mu_{(x,y,\omega)} > 0]$ in free space away from the interface (despite free space's gaplessness) is a measure of the resonances' topological protection.

The spectral localizer's dependence on the choice of κ in Eq. (1) can initially appear problematic. Indeed, for $\kappa = 0$, $L_{(x,y,\omega)}$ is block-diagonal, and its spectrum is always evenly partitioned such that $C^{\mathrm{L}} = 0$. Conversely, for $\kappa \gg 1$, $L_{(x,y,\omega)}$ simply reveals the (exact) joint spectrum of X and Y. However, in between these two limits there is a broad range of κ over which a material's topological properties can be correctly predicted and remain effectively constant. In insulators, such a range always exists [44]. Moreover, in practice we find for our model system that κ can be varied over more than 2 orders of magnitude while $C^{\mathrm{L}}_{(x,y,\omega)}$ remains unaffected and $\mu_{(x,y,\omega)}$ only varies over a factor of 2; see Supplemental Material [58].

Having shown that the chiral edge resonances seen in Fig. 2 are of topological origin, we now demonstrate their topological protection. In general, a system's topology at x, y, ω cannot change without $\mu_{(x,y,\omega)} \to 0$, as the local gap must close for one (or more) of the spectral localizer's eigenvalues to cross the imaginary axis. For Hermitian systems, one can prove that for a system perturbation δH to close the local gap $\mu_{(x,y,\omega)}(X, Y, H + \delta H) = 0$, this perturbation must be at least as strong as the local gap is wide $\|\delta H\| \geq \mu_{(x,y,\omega)}(X, Y, H)$ [43,67]. For non-Hermitian line-gapped systems, this same criteria approximately holds [46]. However, this known limit is not useful for evaluating the topological protection of photonic systems. The problem is that Maxwell's equations (prior to discretization) represent an unbounded operator, for which the ℓ^2 norm is undefined. Thus, after discretization, even relatively modest perturbations will generally still yield substantial changes in the eigen frequency of at least one high frequency state, yielding a large $\|\delta H\|$. Intuitively, the challenge is that $\mu_{(x,y,\omega)}$ is a local measure of protection in both position and frequency, yet $\|\delta H\|$ is a global measure of the perturbation.

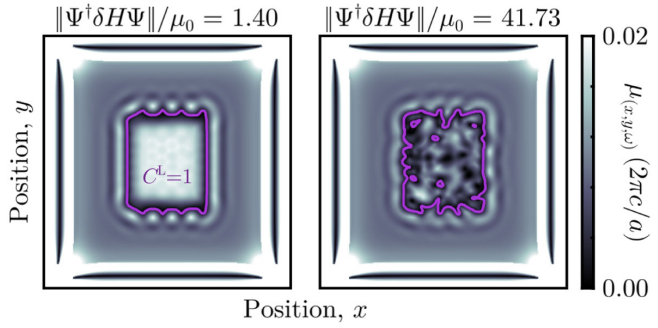

FIG. 3. Local gap and overlaid topological marker ($C^{\mathrm{L}} = 1$ bounded by a magenta line) for the system shown in Fig. 2(a) with added disorder with strengths $\|\Psi^\dagger \delta H \Psi\|/\mu_0 = 1.40$ (left) and $\|\Psi^\dagger \delta H \Psi\|/\mu_0 = 41.73$ (right) relative to the local gap at the center of the ordered system $\mu_0 = 0.0185(2\pi c/a)$. Disorder has been added to the high dielectric rod positions and dimensions and the disorder strength is calculated using the $m = 370$ eigenvectors of H closest to ω; see Supplemental Material [58]. Both figures are shown using the same spatial scale as Fig. 2(d), with $\omega = 0.37(2\pi c/a)$ and $\kappa = 0.04(2\pi c/a^2)$.

Here, we conjecture that a correct measure of a perturbation's local strength is to project it into a subspace near x, y, ω. For our model system, let Ψ be an n-by-m matrix whose m columns are the eigenvectors of H (which is n by n) with eigenvalues that are closest to ω where $\mu_{(x,y,\omega)}$ is calculated. Then, the local marker at x, y, ω cannot change so long as $\|\Psi^\dagger \delta H \Psi\| \lesssim \mu_{(x,y,\omega)}(X, Y, H)$. Note, this conjectured criteria is a necessary but not sufficient condition. For example, changes to the high-dielectric rods' positions and ellipticity require a substantially stronger perturbation to change the system's local topology (Fig. 3). In contrast, removing the external magnetic field, $\nu = 0$ in $\varepsilon_{\mathrm{mo}}$, makes the full system topologically trivial and corresponds to $\|\Psi^\dagger \delta H \Psi\|/\mu_0 = 1.81$, nearly saturating the conjectured bound.

Beyond predicting a system's topological protection against crystal imperfections, the spectral localizer can also be used to approximate a system's robustness to surface roughness. In particular, while crystal imperfections serve to decrease the system's bulk band gap, the effects of which can be captured using topological band theory, the dominant effect of surface roughness is to increase a system's radiative outcoupling. Thus, surface roughness cannot be considered without having a measure of topological protection for heterostructures lacking a global band gap. Here, we artificially increase our model system's radiative outcoupling by increasing the dielectric constant of the surrounding free space environment $\varepsilon_{\mathrm{fs}}$. As can be seen in Fig. 4(a), even for values of $\varepsilon_{\mathrm{fs}}$ greater than any material in the photonic Chern insulator, the spectral localizer is still able to predict the topology of the crystal, as

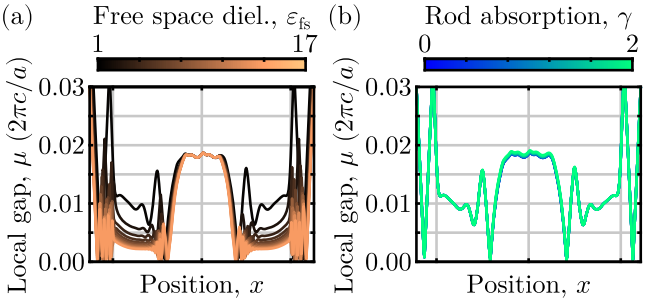

FIG. 4. (a) Local gap for the system shown in Fig. 2(a) for increasing values of the free space environment's dielectric ε_{fs}. (b) Similar to (a), except for increasing values of material absorption in the high-dielectric rods of the photonic Chern insulator, $\varepsilon_{rod} = 14 + i\gamma$, and with $\varepsilon_{fs} = 1$. Both figures are plotted along the green path in Fig. 2(d), with $\omega = 0.37(2\pi c/a)$ and $\kappa = 0.04(2\pi c/a^2)$.

well as the decreasing robustness of the chiral edge state. Given the connection between $\mu_{(x,y,\omega)}$ and the approximate joint spectrum of the system's operators, the decreasing local gap outside of the system for increasing ε_{fs} is a manifestation of the increasing support of the chiral edge resonances outside of the photonic crystal (i.e., decreasing localization). Moreover, the appearance of extra zeros in the local gap near the interface for increasing ε_{fs} is showing that additional, topologically trivial modes are likely appearing at the boundary of the photonic crystal, and these would serve to undermine the transport properties of the chiral edge resonance by allowing for backscattering (see also Fig. S5 in the Supplemental Material [58]). In contrast, if one instead approximates radiative outcoupling as material absorption, the topological protection of the chiral edge resonances is overestimated, as this approximation does not properly capture the salient physics that the system's chiral edge resonances are leaking out of its boundaries [Fig. 4(b)] (still calculated for $\omega \in \mathbb{R}$ to correspond to the topological protection at an observable frequency).

In conclusion, we have shown that gapless topological heterostructures still exhibit bulk-boundary correspondence despite the absence of a global band gap and have demonstrated how to determine the protection of the resulting interface-localized resonances in radiative environments. Moreover, the spectral localizer reveals that treating radiative outcoupling as material absorption overestimates a system's topological protection. As the study of topological photonics turns toward developing devices for specific applications, the spectral localizer's ability to accurately predict topological robustness in radiative environments may enable new photonic device designs that are better protected against radiative outcoupling. Although we have presented this classification approach in a photonic systems, it is broadly applicable to topological materials in general, and in the Supplemental Material we provide examples of using the spectral localizer to classify topology in gapless heterostructures formed from tight-binding models [58].

A. C., T. L., and K. Y. D. acknowledge support from the Laboratory Directed Research and Development program at Sandia National Laboratories. T. L. acknowledges support from the National Science Foundation, Grant No. DMS-2110398. K. Y. D. acknowledges support from the U.S. Department of Energy, Office of Basic Energy Sciences, Division of Materials Sciences and Engineering (BES 20-017574). This work was performed, in part, at the Center for Integrated Nanotechnologies, an Office of Science User Facility operated for the U.S. Department of Energy (DOE) Office of Science. Sandia National Laboratories is a multimission laboratory managed and operated by National Technology and Engineering Solutions of Sandia, LLC, a wholly owned subsidiary of Honeywell International, Inc., for the U.S. DOE's National Nuclear Security Administration under Contract No. DE-NA-0003525. The views expressed in the article do not necessarily represent the views of the U.S. DOE or the United States Government.

*kydixon@sandia.gov
†awcerja@sandia.gov

[1] L. Lu, J. D. Joannopoulos, and M. Soljačić, Topological photonics, Nat. Photonics **8**, 821 (2014).
[2] A. B. Khanikaev and G. Shvets, Two-dimensional topological photonics, Nat. Photonics **11**, 763 (2017).
[3] T. Ozawa, H. M. Price, A. Amo, N. Goldman, M. Hafezi, L. Lu, M. C. Rechtsman, D. Schuster, J. Simon, O. Zilberberg, and I. Carusotto, Topological photonics, Rev. Mod. Phys. **91**, 015006 (2019).
[4] B. Bahari, A. Ndao, F. Vallini, A. E. Amili, Y. Fainman, and B. Kanté, Nonreciprocal lasing in topological cavities of arbitrary geometries, Science **358**, 636 (2017).
[5] P. St-Jean, V. Goblot, E. Galopin, A. Lemaître, T. Ozawa, L. Le Gratiet, I. Sagnes, J. Bloch, and A. Amo, Lasing in topological edge states of a one-dimensional lattice, Nat. Photonics **11**, 651 (2017).
[6] M. A. Bandres, S. Wittek, G. Harari, M. Parto, J. Ren, M. Segev, D. N. Christodoulides, and M. Khajavikhan, Topological insulator laser: Experiments, Science **359**, eaar4005 (2018).
[7] Y. Zeng, U. Chattopadhyay, B. Zhu, B. Qiang, J. Li, Y. Jin, L. Li, A. G. Davies, E. H. Linfield, B. Zhang, Y. Chong, and Q. J. Wang, Electrically pumped topological laser with valley edge modes, Nature (London) **578**, 246 (2020).
[8] Z.-Q. Yang, Z.-K. Shao, H.-Z. Chen, X.-R. Mao, and R.-M. Ma, Spin-momentum-locked edge mode for topological vortex lasing, Phys. Rev. Lett. **125**, 013903 (2020).
[9] Z.-K. Shao, H.-Z. Chen, S. Wang, X.-R. Mao, Z.-Q. Yang, S.-L. Wang, X.-X. Wang, X. Hu, and R.-M. Ma, A high-performance topological bulk laser based on band-inversion-induced reflection, Nat. Nanotechnol. **15**, 67 (2020).

[10] B. Bahari, L. Hsu, S. H. Pan, D. Preece, A. Ndao, A. El Amili, Y. Fainman, and B. Kanté, Photonic quantum Hall effect and multiplexed light sources of large orbital angular momenta, Nat. Phys. **17**, 700 (2021).

[11] A. Dikopoltsev, T. H. Harder, E. Lustig, O. A. Egorov, J. Beierlein, A. Wolf, Y. Lumer, M. Emmerling, C. Schneider, S. Höfling, M. Segev, and S. Klembt, Topological insulator vertical-cavity laser array, Science **373**, 1514 (2021).

[12] L. Yang, G. Li, X. Gao, and L. Lu, Topological-cavity surface-emitting laser, Nat. Photonics **16**, 279 (2022).

[13] M. C. Rechtsman, Y. Lumer, Y. Plotnik, A. Perez-Leija, A. Szameit, and M. Segev, Topological protection of photonic path entanglement, Optica **3**, 925 (2016).

[14] S. Barik, A. Karasahin, C. Flower, T. Cai, H. Miyake, W. DeGottardi, M. Hafezi, and E. Waks, A topological quantum optics interface, Science **359**, 666 (2018).

[15] S. Mittal, E. A. Goldschmidt, and M. Hafezi, A topological source of quantum light, Nature (London) **561**, 502 (2018).

[16] S. Barik, A. Karasahin, S. Mittal, E. Waks, and M. Hafezi, Chiral quantum optics using a topological resonator, Phys. Rev. B **101**, 205303 (2020).

[17] N. Parappurath, F. Alpeggiani, L. Kuipers, and E. Verhagen, Direct observation of topological edge states in silicon photonic crystals: Spin, dispersion, and chiral routing, Sci. Adv. **6**, eaaw4137 (2020).

[18] S. Arora, T. Bauer, R. Barczyk, E. Verhagen, and L. Kuipers, Direct quantification of topological protection in symmetry-protected photonic edge states at telecom wavelengths, Light Sci. Appl. **10**, 9 (2021).

[19] T. Dai, Y. Ao, J. Bao, J. Mao, Y. Chi, Z. Fu, Y. You, X. Chen, C. Zhai, B. Tang, Y. Yang, Z. Li, L. Yuan, F. Gao, X. Lin, M. G. Thompson, J. L. O'Brien, Y. Li, X. Hu, Q. Gong, and J. Wang, Topologically protected quantum entanglement emitters, Nat. Photonics **16**, 248 (2022).

[20] N. V. Hauff, H. Le Jeannic, P. Lodahl, S. Hughes, and N. Rotenberg, Chiral quantum optics in broken-symmetry and topological photonic crystal waveguides, Phys. Rev. Res. **4**, 023082 (2022).

[21] M. Z. Hasan and C. L. Kane, Colloquium: Topological insulators, Rev. Mod. Phys. **82**, 3045 (2010).

[22] X.-L. Qi and S.-C. Zhang, Topological insulators and superconductors, Rev. Mod. Phys. **83**, 1057 (2011).

[23] A. Bansil, H. Lin, and T. Das, Colloquium: Topological band theory, Rev. Mod. Phys. **88**, 021004 (2016).

[24] C.-K. Chiu, J. C. Y. Teo, A. P. Schnyder, and S. Ryu, Classification of topological quantum matter with symmetries, Rev. Mod. Phys. **88**, 035005 (2016).

[25] Z. Wang, Y. Sun, X.-Q. Chen, C. Franchini, G. Xu, H. Weng, X. Dai, and Z. Fang, Dirac semimetal and topological phase transitions in A_3Bi (A = Na, K, Rb), Phys. Rev. B **85**, 195320 (2012).

[26] Z. K. Liu, B. Zhou, Y. Zhang, Z. J. Wang, H. M. Weng, D. Prabhakaran, S.-K. Mo, Z. X. Shen, Z. Fang, X. Dai, Z. Hussain, and Y. L. Chen, Discovery of a three-dimensional topological Dirac semimetal, Na3Bi, Science **343**, 864 (2014).

[27] Z. Wang, H. Weng, Q. Wu, X. Dai, and Z. Fang, Three-dimensional Dirac semimetal and quantum transport in Cd_3As_2, Phys. Rev. B **88**, 125427 (2013).

[28] H. Weng, C. Fang, Z. Fang, B. A. Bernevig, and X. Dai, Weyl semimetal phase in noncentrosymmetric transition-metal monophosphides, Phys. Rev. X **5**, 011029 (2015).

[29] B. Q. Lv, N. Xu, H. M. Weng, J. Z. Ma, P. Richard, X. C. Huang, L. X. Zhao, G. F. Chen, C. E. Matt, F. Bisti, V. N. Strocov, J. Mesot, Z. Fang, X. Dai, T. Qian, M. Shi, and H. Ding, Observation of Weyl nodes in TaAs, Nat. Phys. **11**, 724 (2015).

[30] L. Lu, Z. Wang, D. Ye, L. Ran, L. Fu, J. D. Joannopoulos, and M. Soljačić, Experimental observation of Weyl points, Science **349**, 622 (2015).

[31] M. Xiao, W.-J. Chen, W.-Y. He, and C. T. Chan, Synthetic gauge flux and Weyl points in acoustic systems, Nat. Phys. **11**, 920 (2015).

[32] F. Li, X. Huang, J. Lu, J. Ma, and Z. Liu, Weyl points and Fermi arcs in a chiral phononic crystal, Nat. Phys. **14**, 30 (2018).

[33] B. Xie, H. Liu, H. Cheng, Z. Liu, S. Chen, and J. Tian, Experimental realization of type-II Weyl points and fermi arcs in phononic crystal, Phys. Rev. Lett. **122**, 104302 (2019).

[34] Y. Yang, H.-x. Sun, J.-p. Xia, H. Xue, Z. Gao, Y. Ge, D. Jia, S.-q. Yuan, Y. Chong, and B. Zhang, Topological triply degenerate point with double Fermi arcs, Nat. Phys. **15**, 645 (2019).

[35] A. A. Burkov, M. D. Hook, and L. Balents, Topological nodal semimetals, Phys. Rev. B **84**, 235126 (2011).

[36] Q. Xu, Z. Song, S. Nie, H. Weng, Z. Fang, and X. Dai, Two-dimensional oxide topological insulator with iron-pnictide superconductor LiFeAs structure, Phys. Rev. B **92**, 205310 (2015).

[37] B.-B. Fu, C.-J. Yi, T.-T. Zhang, M. Caputo, J.-Z. Ma, X. Gao, B. Lv, L.-Y. Kong, Y.-B. Huang, P. Richard *et al.*, Dirac nodal surfaces and nodal lines in ZrSiS, Sci. Adv. **5**, eaau6459 (2019).

[38] F. D. M. Haldane and S. Raghu, Possible realization of directional optical waveguides in photonic crystals with broken time-reversal symmetry, Phys. Rev. Lett. **100**, 013904 (2008).

[39] S. Raghu and F. D. M. Haldane, Analogs of quantum-Hall-effect edge states in photonic crystals, Phys. Rev. A **78**, 033834 (2008).

[40] *Advances in FDTD Computational Electrodynamics: Photonics and Nanotechnology*, edited by A. Taflove, A. Oskooi, and S. G. Johnson, Artech House Antennas and Propagation Series (Artech House, Boston, 2013), oCLC: ocn811964793.

[41] M. C. Rechtsman, J. M. Zeuner, Y. Plotnik, Y. Lumer, D. Podolsky, F. Dreisow, S. Nolte, M. Segev, and A. Szameit, Photonic Floquet topological insulators, Nature (London) **496**, 196 (2013).

[42] M. Hafezi, S. Mittal, J. Fan, A. Migdall, and J. M. Taylor, Imaging topological edge states in silicon photonics, Nat. Photonics **7**, 1001 (2013).

[43] T. A. Loring, K-theory and pseudospectra for topological insulators, Ann. Phys. (Amsterdam) **356**, 383 (2015).

[44] T. A. Loring and H. Schulz-Baldes, Finite volume calculation of K-theory invariants, New York J. Math. **23**, 1111 (2017), http://nyjm.albany.edu/j/2017/23-48.html.

[45] T. A. Loring and H. Schulz-Baldes, The spectral localizer for even index pairings, J. Noncommut. Geom. **14**, 1 (2020).
[46] A. Cerjan, L. Koekenbier, and H. Schulz-Baldes, Spectral localizer for line-gapped non-hermitian systems, J. Math. Phys. (N.Y.) **64**, 082102 (2023).
[47] A. Cerjan, T. A. Loring, and F. Vides, Quadratic pseudospectrum for identifying localized states, J. Math. Phys. (N.Y.) **64**, 023501 (2023).
[48] A. Kitaev, Periodic table for topological insulators and superconductors, AIP Conf. Proc. **1134**, 22 (2009).
[49] M.-D. Choi, Almost commuting matrices need not be nearly commuting, Proc. Am. Math. Soc. **102**, 529 (1988).
[50] A. Kitaev, Anyons in an exactly solved model and beyond, Ann. Phys. (Amsterdam) **321**, 2 (2006).
[51] A. P. Schnyder, S. Ryu, A. Furusaki, and A. W. W. Ludwig, Classification of topological insulators and superconductors in three spatial dimensions, Phys. Rev. B **78**, 195125 (2008).
[52] A. Kitaev, Periodic table for topological insulators and superconductors, AIP Conf. Proc. **1134**, 22 (2009).
[53] S. Ryu, A. P. Schnyder, A. Furusaki, and A. W. W. Ludwig, Topological insulators and superconductors: Tenfold way and dimensional hierarchy, New J. Phys. **12**, 065010 (2010).
[54] W. Cheng, A. Cerjan, S.-Y. Chen, E. Prodan, T. A. Loring, and C. Prodan, Revealing topology in metals using experimental protocols inspired by K-theory, Nat. Commun. **14**, 3071 (2023).
[55] A. Cerjan and T. A. Loring, An operator-based approach to topological photonics, Nanophotonics **11**, 4765 (2022).
[56] K. Yee, Numerical solution of initial boundary value problems involving Maxwell's equations in isotropic media, IEEE Trans. Antennas Propag. **14**, 302 (1966).
[57] A. Cerjan, acerjan/spectral_localizer_radiative_photonic_crystal (2023), original-date: 2023-07-01T22:09:33Z.
[58] See Supplemental Material, which includes Refs. [59–66], at http://link.aps.org/supplemental/10.1103/PhysRevLett.131.213801 for details on the allowable range of κ, a discussion of the numerical calculation of the local Chern number in non-Hermitian systems, and an example of using the spectral localizer to classify the topology of a gapless tight-binding heterostructure. The Supplemental Material also contains an archived version of the implementation of the spectral localizer for Maxwell's equations.
[59] J. Sylvester, XIX. A demonstration of the theorem that every homogeneous quadratic polynomial is reducible by real orthogonal substitutions to the form of a sum of positive and negative squares, London, Edinburgh, Dublin Philos. Mag. J. Sci. **4**, 138 (1852).
[60] N. J. Higham, Sylvester's influence on applied mathematics, Math. Today Bull. Inst. Math. Appl. **50**, 202 (2014), https://eprints.maths.manchester.ac.uk/2142/.
[61] F. D. M. Haldane, Model for a quantum Hall effect without landau levels: Condensed-matter realization of the "parity anomaly", Phys. Rev. Lett. **61**, 2015 (1988).
[62] D. L. Bergman and G. Refael, Bulk metals with helical surface states, Phys. Rev. B **82**, 195417 (2010).
[63] A. Junck, K. W. Kim, D. L. Bergman, T. Pereg-Barnea, and G. Refael, Transport through a disordered topological-metal strip, Phys. Rev. B **87**, 235114 (2013).
[64] A. Cerjan and T. A. Loring, Local invariants identify topology in metals and gapless systems, Phys. Rev. B **106**, 064109 (2022).
[65] H. Shen, B. Zhen, and L. Fu, Topological band theory for non-Hermitian Hamiltonians, Phys. Rev. Lett. **120**, 146402 (2018).
[66] A. Li, H. Wei, M. Cotrufo, W. Chen, S. Mann, X. Ni, B. Xu, J. Chen, J. Wang, S. Fan, C.-W. Qiu, A. Alù, and L. Chen, Exceptional points and non-Hermitian photonics at the nanoscale, Nat. Nanotechnol. **18**, 706 (2023).
[67] R. Bhatia, *Matrix Analysis*, Graduate Texts in Mathematics Vol. 169 (Springer, New York, New York, NY, 1997), 10.1007/978-1-4612-0653-8.